DJS Vol. 48(1)(2024) pp. 186-206 ISSN: 1012-5965

Delta Journal of Science
Available online at
https://djs.journals.ekb.eg/

Research Article

MATHEMATICS

Design of backpropagation learning algorithm for MHD mixed convective Prandtl nanofluid flow with activation energy

Eman Fayz A. Alshehery*[1], Eman Salem Alaidarous[1], Rania. A. Alharbey[1], Muhammad Asif Zahoor Raja[2]

[1]Department of Mathematics, Faculty of Science, King Abdulaziz University, Jeddah 21589, Saudi Arabia
[2]Future Technology Research Center, National Yunlin University of Science and Technology, Douliou, Yunlin 64002, Taiwan

***Corresponding author:** Eman Fayz A. Alshehery **Email:** eabdulrahmanalshehery@stu.kau.edu.sa

Received: 8/3/2024 **Accepted:** 23 /3/2024

KEY WORDS

Activation Energy, Prandtl Nanofluid, Artificial Neural Network, Lobatto IIIA, Levenberg Marquardt, MHD.

ABSTRACT

The use of artificial intelligence techniques for solving challenges has grown in popularity recently in a range of areas. Additionally, nanofluid is interesting for a variety of applications, especially in cooling and heat transfer systems, since it is used to improve the thermal features of fluid. In the present study, a design of a backpropagation learning algorithm is provided to analyze the flow properties in a magnetohydrodynamic mixed convective flow of Prandtl nanofluid (MHD-MCPNFF) with gyrotactic microorganisms over a stretchable surface affected by the activation energy. An ordinary differential equations ODEs system is obtained from a partial differential equations PDEs system of the original mathematical formulation by using suitable transformations. Applying the Lobatto IIIA technique to solve ODEs for various scenarios by changing the values of Prandtl fluid parameter (α), magnetic parameter (M), Brownian motion (Nb), thermophoresis (Nt), activation energy (E), chemical reaction rate (σ), and Peclet number (Pe) to find a set of data for the MHD-MCPNFF model. Using these solutions through nftool in MATLAB for designing the Levenberg–Marquardt backpropagation learning algorithm (LMBLA). The effectiveness and accuracy of the designed LMBLA are verified through the mean squared error (MSE), error histograms, and regression illustration plots. The flow velocity has the opposite behavior for growing values for Prandtl fluid and magnetic parameters. For rising values of Brownian motion and thermophoresis parameters, the fluid temperature increases. The increasing values of the activation energy parameter imply the increasing concentration of nanoparticles

Introduction

A fluid that includes nanoparticles, or particles smaller than a nanometer, is referred to as a nanofluid. Nanofluid is created by a small number of nanoparticles as metals or oxides pendant in traditional fluids such as water and oil. Nanofluids have superior thermal features useful in a wide range of heat transfer applications, such as coolants in many types of heat transfer devices, including radiators and electronic cooling systems. Actually, Choi and Eastmen (1995) presented the first study to use the term "nanofluid". Recently, many studies have investigated nanofluid mechanics. Al-Yaari et al., (2023) developed a model to evaluate the influence of nanofluid thermophysical properties in a heterogeneous porous media to enhance oil recovery. The impact of nanofluid type, nanoparticle concentration, and nanofluid depths on solar still performance was investigated by (Modi et al., 2023) using up-to-date literature. By evaluating the viscosity and thermal conductivity of magnet nanofluids (Selim et al., 2023) examined the effects of an external magnetic field on nanofluids. Hafeez et al., (2023) researched the impact of Cu-Al2O3 nanoparticles on the rheological, dynamic viscosity, and thermal conductivity of kerosene oil-based hybrid nanofluids .

The exploration of the dynamics of fluids that conduct electricity is known as magnetohydrodynamics (MHD). It derives from magneto, which means magnetic field, and hydro, which means water, and also dynamics, which means movement. MHD is used widely in industry and engineering but is largely employed in nanotechnology. In recent decades, many researchers studied the features of MHD. In the presence of an angled magnetization and viscous dissipation, (Galal et al., 2024) explored the transfer rate of heat and mass for three-dimensional MHD nanofluid flow with thermal radiation and chemical reaction across the dual stretchable surface. Based on the MHD non-Newtonian (Maxwell) nanofluid flow with anArrhenius activation energy, (Ahmed et al., 2024) investigated both linear and nonlinear radiation patterns. Mahmood et al., (2023) studied the effects of mass suction and heat production/abstraction on MHD stagnation point flow in a nonlinearly shrinking/stretching sheet of a water-based tri-hybrid nanofluid. In the presence of internal heat generation and a sink, (Reddy et al., 2023) evaluated the effects of the MHD heat transfer features of an incompressible viscous fluid over a constantly stretching horizontal cylinder submerged in a porous medium.

A theoretical structure called the Prandtl fluid model is employed to explain the dynamics of fluids with certain properties, especially those that have poor thermal conductivity and high viscosity. It takes the name of the German researcher and engineer Ludwig Prandtl who made important advances in fluid mechanics. Many engineering issues have been addressed using it, such as the investigation of heat transport close to solid surfaces and the aerodynamics of airfoils. In the flow of MHD Prandtl fluid along an unsteady stretched surface (Asad and Riaz, 2023) assessed entropy production using Soret and Dufour impact. The Prandtl-Eyring nanofluid was researched by (Shah et al., 2023) with base fluid motor oil passing across a heated stretching surface with the generation of entropy.

The rate of chemical changes can vary depending on several factors, such as activation energy and it can be used to understand the entire process and the reaction mechanism. In 1889, the scientist Arrhenius first put up the concept "activation energy". As the name implies, it is the least amount of energy desired to initiate a chemical process or mimic a reaction. Very few investigations have been conducted on the chemical process and activation energy. Bio-convected unstable Williamson fluid flow at a heated stretching surface in a porous medium was studied numerically by (Jabeen et al., 2024). The research also examined the presence of specific viscous dissipation and activation energy. Waqas et al., (2023) investigated numerically the micropolar nanofluid flow over a three-dimensional rotating surface, including activation energy and heat source/sink influences throughout the rotating surface. Jawad et al., (2023) addressed the convective Darcy-Forchheimer flow of the Maxwell nanofluid via a porous stretched sheet and the effects of activation energy and mass transfer. Yasir et al. (2023) observed the impact of activation energy on the micro-rotation characteristics of magnetized micropolar fluid flow at the stagnation point region on a porous shrinking surface harboring gyrotactic microorganisms .

The artificial neural network (ANN) is a normal statistical method for analyzing the correlations between variables. An ANN is designed of continuous layers of different nodes that analyze input and provide outputs depending on activation functions that have been predetermined. One popular supervised learning technique for artificial neural network training is backpropagation. In 1974, Paul Werbos invented the backpropagation technique. Backpropagation uses the gradient descent technique, which minimizes network error. Generally, backpropagation learning algorithms are used for this such as the Levenberg–Marquardt backpropagation

learning algorithm LMBLA which is designed and used in this paper. Using Levenberg-Marquardt backpropagation neural networks, (Asghar et al., 2024) presented the numerical solutions to singular functional delay differential equations of third, fourth, and fifth orders, which occur in quantum calculus models. Goud et al., (2023) investigated the non-Fourier unsteady heat transference of a trapezoidal porous fin by using the Levenberg-Marquardt technique of backpropagation artificial neural network to study the thermal variations in the fin. Mukdasai et al., (2022) used the effectiveness of stochastic numerical supervised neural networks to show numerical simulations of the novel fractional order Leptospirosis model.

To the authors' best knowledge, all previously published studies are limited to using the traditional numerical treatments to solve stiff nonlinear equations systems for flow models of nanofluidic problems. Consequently, this study lists the primary contributions to designing a backpropagation learning algorithm based on the Levenberg-Marquardt backpropagation learning algorithm LMBLA through the nftool package in MATLAB and it uses to find the numerical solution for a magnetohydrodynamic mixed convective flow of Prandtl nanofluid (MHD-MCPNFF) with gyrotactic microorganisms over a stretchable surface affected by the activation energy. Also, current study used the numerical and graphical statistical data to verify the success and precision of this new algorithm to use it for predicting problem solutions in various fields. Furthermore, this study provided numerical solutions of the MHD-MCPNFF model by LMBLA are used to examine the variants of flow dynamics such as flow velocity, fluid temperature, nanoparticle concentration, and microorganisms motile density by changing values of specific physical parameters.

Nomenclature:

MHD	Magnetohydrodynamics
ANN	Artificial neural network
LMBLA	Levenberg Marquardt backpropagation learning algorithm
ODE	Ordinary differential equations
T_w	Fixed temperature
C_w	Fixed concentration
Ω_w	Fixed motile density
ν	kinematic viscosity
Gr	Grashof number
g	Gravitational acceleration
W_c	Local Weissenberg number
MCPNFF	Mixed convective flow of Prandtl nanofluid
(x, y)	Cartesian coordinates
PDE	Partial differential equations
MSE	Mean squared error
Ω_∞	Free motile density
T_∞	Free flow temperature
C_∞	Free flow concentration
α^*	Thermal diffusivity
K_r	Chemical reaction constant
m	Fitted rate constant
S1 *C1*	Scenario 1,…, etc Case 1,…, etc

Model of the problem

The model of the problem can be seen in Fig. (1). Here, let us suppose an incompressible MHD mixed convective flow of Prandtl nanofluid in the presence of microorganisms with the impact of activation energy across a stretchable surface. Consider in this problem the following

- The velocity components are u and v in the x-direction and y-direction, respectively along the stretching surface.
- T, C, and Ω represent the fluid temperature, nanoparticle concentration, and microorganism density close to the surface, respectively.
- For the present model flow, the additional stress tensor was defined as (Kumar et al., 2017).

$$\tau = \frac{c_1 \sin^{-1}\left(\frac{1}{c_2}\left[\left(\frac{\partial u}{\partial y}\right)^2 + \left(\frac{\partial v}{\partial y}\right)^2\right]^{1/2}\right)}{\left[\left(\frac{\partial u}{\partial y}\right)^2 + \left(\frac{\partial v}{\partial y}\right)^2\right]^{1/2}} \frac{\partial u}{\partial y}$$

Where (c_1, c_2) represent the material variable of the Prandtl fluid model.

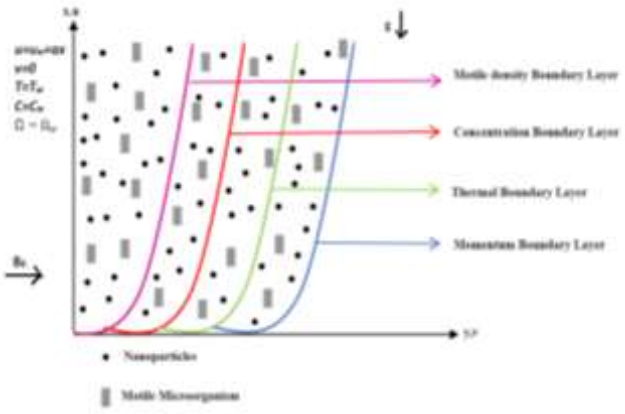

Fig. (1): The problem geometry

The governing PDEs for the suggested flow model are (Zafar et al., 2023).

$$\frac{\partial u}{\partial x} + \frac{\partial v}{\partial y} = 0, \quad (1)$$

$$u\frac{\partial u}{\partial x} + v\frac{\partial v}{\partial y} = \upsilon\frac{c_1}{c_2}\frac{\partial^2 u}{\partial y^2} + \frac{\upsilon c_1}{2c_2^3}\left(\frac{\partial u}{\partial y}\right)^2\frac{\partial^2 u}{\partial y^2} - \frac{\omega B_0^2}{\rho}u + g\beta(1-C_\infty)(T-T_\infty) - g\left[\frac{\rho_p - \rho_f}{\rho_f}\right](C-C_\infty) - \gamma_1 g\left[\frac{\rho_m - \rho_f}{\rho_f}\right](\Omega - \Omega_\infty), \quad (2)$$

$$u\frac{\partial T}{\partial x} + v\frac{\partial T}{\partial y} = \alpha^*\frac{\partial^2 T}{\partial y^2} + \tau^*\left(D_B\frac{\partial C}{\partial y}\frac{\partial T}{\partial y} + \frac{D_T}{T_\infty}\left(\frac{\partial T}{\partial y}\right)^2\right), \quad (3)$$

$$u\frac{\partial C}{\partial x} + v\frac{\partial C}{\partial y} = D_B\left(\frac{\partial^2 C}{\partial y^2}\right) + \frac{D_T}{T_\infty}\left(\frac{\partial^2 T}{\partial y^2}\right) - K_r^2\left(\frac{T}{T_\infty}\right)^m exp\left(-\frac{E_a}{K_1 T}\right)(C-C_\infty), \quad (4)$$

$$u\frac{\partial \Omega}{\partial x} + v\frac{\partial \Omega}{\partial y} + bW_c\frac{\partial}{\partial y}\left(\frac{\Omega}{C_w - C_\infty}\frac{\partial C}{\partial y}\right) = D_m\frac{\partial^2 \Omega}{\partial y^2}, \quad (5)$$

The boundary conditions are

$$u = u_w = ax,\ v = 0,\ T = T_w,\ C = C_w,\ \Omega = \Omega_w, \text{ at } y = 0, \quad (6)$$

$$u \to 0,\ T \to T_\infty,\ C \to C_\infty,\ \Omega \to \Omega_\infty \text{ as } z \to \infty. \quad (7)$$

where ρ is the fluid electrical conductivity, α^* is the fluid thermal diffusivity, υ is the fluid kinematic viscosity, E_a is the activation energy, τ^* is the particle heat capacity to the fluid heat capacity, D_T, D_B, and D_m are the thermophoretic, Brownian motion, and microorganism diffusion parameters, respectively.

Using the dimensionless variables

$$\eta = y\sqrt{\frac{a}{\upsilon}}, \theta(\eta) = \frac{T - T_\infty}{T_w - T_\infty}, \varphi(\eta) = \frac{C - C_\infty}{C_w - C_\infty}, \chi(\eta) = \frac{\Omega - \Omega_\infty}{\Omega_w - \Omega_\infty},$$
$$u = axf'(\eta), v = \sqrt{a\upsilon}[f(\eta)], \psi = \sqrt{a\upsilon}[xf(\eta)]. \quad (8)$$

This gives the following ODEs

$$af''' - (f')^2 + ff'' + a\beta(f'')^2 f''' - Mf' + \Lambda(\theta - N\varphi - R_b\chi) = 0, \quad (9)$$

$$\theta'' + Pr\left(f\theta' + Nb\theta'\varphi' + Nt\theta'^2\right) = 0, \quad (10)$$

$$\varphi'' + Scf\varphi' + \frac{Nt}{Nb}\theta'' - Sc\sigma\varphi(1+\delta\theta)^m exp\left(-\frac{E}{1+\delta\theta}\right) = 0, \quad (11)$$

$$\chi'' + Lb(f\chi') - Pe[\varphi''(\chi + \lambda) + \chi'\varphi'] = 0. \quad (12)$$

where $\alpha = \frac{c_1}{c_2}$ is the Prandtl fluid parameter, $\beta = \frac{a^3 x^2}{2c^2 \upsilon}$ is the elastic parameter, $M = \frac{\sigma B_0^2}{a\rho}$ is the magnetic parameter, $\Lambda = \frac{Gr}{Re_x^2}$ is the mixed convective parameter, $N = \frac{g\beta_C(C_w - C_\infty)}{g\beta_T(T_w - T_\infty)}$ is the buoyancy ratio parameter, $R_b = \frac{\chi(\rho_m - \rho_f)(\Omega_w - \Omega_\infty)}{\rho_f \beta(1-C_\infty)(T_w - T_\infty)}$ is the bioconvection Rayleigh number, $Pr = \frac{\delta}{\alpha}$ is the Prandtl number, $Nb = \frac{\tau D_B \Delta C}{\upsilon}$ is Brownian motion parameter, $Nt = \frac{\tau D_T \Delta T}{\upsilon T_\infty}$ is thermophoresis parameter, $Sc = \frac{\upsilon}{D_B}$ is Schmidt number, $\sigma = \frac{K_r^2}{a}$ is chemical reaction parameter $\delta = \frac{T_w - T_\infty}{T_\infty}$ is temperature ratio, m is fitted rate parameter which it lies in the range $-1 < m < 1$, $E = \frac{E_a}{K_1 T_\infty}$ is activation energy constant, $Lb = \frac{\upsilon}{D_m}$ is the bioconvection Lewis number, $Pe = \frac{bW_c}{D_m}$ is the Peclet number, and $\lambda = \frac{N_\infty}{N_w - N_\infty}$ is the motile microbes parameter.

Boundary conditions as

$$f'(0) = 1, f(0) = 0, \varphi(0) = \theta(0) = \chi(\eta) = 1, \text{ at } \eta = 0, \quad (13)$$

$$f'(\infty) = 0, \theta(\infty) = 0 = \varphi(\infty), \chi(\infty) = 0. \text{ as } \eta \to \infty. \quad (14)$$

Additionally, the physical quantities are (Bafakech et al., 2022)

$$Cf_x = \frac{\tau_w}{\rho u_w^2}, Nu_x = \frac{x q_w}{K_1(T_w - T_\infty)}, Sh_x = \frac{x q_m}{D_B(C_w - C_\infty)}, Nn_x = \frac{x q_n}{D_m(\Omega_w - \Omega_\infty)}. \quad (15)$$

where Cf_x is the skin friction coefficient, τ_w is shear stress, Nu_x is the local Nusselt number, q_w is the surface heat flux, Sh_x is the local Sherwood number, q_m is the surface mass flux, Nn_x is the local density of microorganism, and q_n is the motile microorganism flux. Therefore

$$\tau_w = \frac{c_1 \partial u}{c_2 \partial y} + \frac{c_1}{6c_2^3}\left(\frac{\partial u}{\partial y}\right)^3, q_w = -K_1 \frac{\partial T}{\partial y}, q_m = -D_B \frac{\partial C}{\partial y}, q_n = -D_m \frac{\partial N}{\partial y}. \quad (16)$$

With these quantities, and the provided similarity transformation,

$$\mu Cf_x (Re_x)^{-1/2} = af'' + \frac{a\beta}{3}(f''')^3, Nu_x (Re_x)^{-1/2} = -\theta'(0), Sh_x (Re_x)^{-1/2} = -\phi'(0), Nn_x (Re_x)^{-1/2} = -\chi'(0). \quad (17)$$

Here, $(Re_x) = \frac{x u_w}{\upsilon}$ represents the local Reynolds number.

Methodology explanation

The backpropagation learning of ANN is regarded as a function optimization problem, in which the aim is to find the ideal network parameters (weights and biases) to minimize neural network error. The Levenberg-Marquardt backpropagation learning algorithm LMBLA is one of several functional optimization techniques that can be directly used in network learning. To design this algorithm, there are two steps: the first step is to find the numerical solutions used to create a dataset for

LMBLA and the other step is the process of applying this algorithm and verifying its accuracy and effectiveness.

The LMBLA data set is the numerical solutions of the dimensionless flow model MHD-MCPNFF represented by ODEs in Eqs. (8)-(12) with Eqs. (13)-(14). Using the Lobatto IIIA approach to find these solutions with the help of MATLAB software. The numerical solutions are determined by input values between 0 and 6, with a 0.001 step size for several scenarios S1-S7 by the changes of physical parameters α, M, Nb, Nt, E, σ, and Pe, each with four cases C1-C4 of MHD-MCPNFF, as explained in Table (1).

The recommended LMBLA methodology is designed to find the numerical treatments of the MHD-MCPNFF model for various scenarios using the command "nftool" through the MATLAB program in the neural network toolbox. For 6001 input points, the data set can be divided as follows:

- 75% of the data set is employed for the training process.
- 15% of the data set is used in the testing process.
- 15% of the data set is utilized for the validation process.

Additionally, the number of neurons is changed to 20 under the required level of accuracy for computing results.

Figure 2 indicates the architecture of the recommended network.

Table (1): Details of scenarios and cases for MHD-MCPNFF

Scenarios	Cases	Physical Quantities						
		α	M	Nb	Nt	E	σ	Pe
1	1	0.1	0.1	0.1	0.1	0.1	0.1	1.0
	2	0.2	0.1	0.1	0.1	0.1	0.1	1.0
	3	0.3	0.1	0.1	0.1	0.1	0.1	1.0
	4	0.4	0.1	0.1	0.1	0.1	0.1	1.0
2	1	0.1	0.1	0.1	0.1	0.1	0.5	1.0
	2	0.1	0.2	0.1	0.1	0.1	0.5	1.0
	3	0.1	0.3	0.1	0.1	0.1	0.5	1.0
	4	0.1	0.4	0.1	0.1	0.1	0.5	1.0
3	1	0.1	0.1	0.1	0.1	0.1	0.1	1.0
	2	0.1	0.1	0.3	0.1	0.1	0.1	1.0
	3	0.1	0.1	0.5	0.1	0.1	0.1	1.0
	4	0.1	0.1	0.7	0.1	0.1	0.1	1.0
4	1	0.1	0.1	1.0	0.1	0.1	0.1	1.0
	2	0.1	0.1	1.0	0.3	0.1	0.1	1.0
	3	0.1	0.1	1.0	0.5	0.1	0.1	1.0
	4	0.1	0.1	1.0	0.7	0.1	0.1	1.0
5	1	0.1	0.1	0.1	0.1	0.1	0.1	1.0
	2	0.1	0.1	0.1	0.1	0.5	0.1	1.0
	3	0.1	0.1	0.1	0.1	1.0	0.1	1.0
	4	0.1	0.1	0.1	0.1	1.5	0.1	1.0
6	1	0.1	0.1	0.1	0.1	0.1	0.1	1.0
	2	0.1	0.1	0.1	0.1	0.1	0.2	1.0
	3	0.1	0.1	0.1	0.1	0.1	0.3	1.0
	4	0.1	0.1	0.1	0.1	0.1	0.4	1.0
7	1	0.1	0.1	0.1	0.1	0.1	0.1	1.0
	2	0.1	0.1	0.1	0.1	0.1	0.1	1.2
	3	0.1	0.1	0.1	0.1	0.1	0.1	1.4
	4	0.1	0.1	0.1	0.1	0.1	0.1	1.6

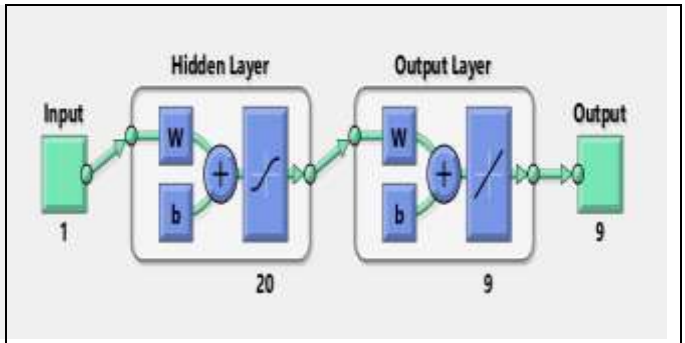

Fig. (2): The architecture of the recommended network

Results and discussion

The effectiveness and accuracy evaluation of LMBLA processes for seven scenarios with varying cases in MHD-MCPNFF through the comparison between target data (solutions by Lobatto IIIA) and output data (solutions by LMBLA), is illustrated graphically in Figs. 3, 4, 5, 6, and 7.

As shown in Table (2), the analysis of all numerical data including MSE for training, testing and validation, performance, gradient, mu, epochs, and time for each of the four cases of the seven scenarios. Table (2) indicates that the MSE performance of the LMBLA processes is in the range (10^{-10} to 10^{-11}). These numerical results demonstrate the best performance of LMBLA in the MHD-MCPNFF solution.

Table (2): Total numerical analysis of LMBLA for MHD-MCPNFF

Scenario	Case	MSE			Performance	Mu	Gradient	Epochs	Time (S)
		Training	**Validation**	**Testing**					
S1	C1	4.36E-10	4.23E-10	4.15E-10	4.36E-10	1.00E-10	9.98E-08	123	22
	C2	9.33E-10	1.00E-09	9.14E-10	9.33E-10	1.00E-09	9.98E-08	431	36
	C3	1.79E-10	1.74E-10	1.87E-10	1.79E-10	1.00E-10	9.89E-08	135	11
	C4	1.87E-10	1.90E-10	1.85E-10	1.87E-10	1.00E-10	9.93E-08	132	11
S2	C1	7.47E-11	6.73E-11	7.92E-11	7.47E-11	1.00E-09	1.68E-08	573	50
	C2	8.52E-11	8.55E-11	8.35E-11	8.52E-11	1.00E-10	9.99E-08	290	23
	C3	1.56E-10	1.61E-10	1.61E-10	1.56E-10	1.00E-09	4.26E-08	141	11
	C4	5.35E-10	4.98E-10	5.49E-10	5.35E-10	1.00E-10	9.85E-08	116	9
S3	C1	3.49E-10	3.26E-10	3.54E-10	3.49E-10	1.00E-10	9.91E-08	131	10
	C2	4.28E-10	4.47E-10	4.43E-10	4.28E-10	1.00E-10	9.79E-08	139	11
	C3	1.91E-11	1.94E-11	1.83E-11	1.91E-11	1.00E-10	9.91E-08	497	43
	C4	3.40E-11	3.44E-11	3.35E-11	3.40E-11	1.00E-10	9.95E-08	540	45
S4	C1	4.45E-10	4.95E-10	4.44E-10	4.45E-10	1.00E-10	9.99E-08	126	10
	C2	1.56E-10	1.59E-10	1.57E-10	1.56E-10	1.00E-09	9.97E-08	664	57
	C3	1.87E-10	1.91E-10	1.97E-10	1.87E-10	1.00E-10	9.85E-08	210	17
	C4	4.96E-11	5.16E-11	4.91E-11	4.96E-11	1.00E-10	9.94E-08	371	31
S5	C1	1.23E-11	1.26E-11	1.28E-11	1.23E-11	1.00E-10	9.93E-08	569	50
	C2	4.07E-11	4.08E-11	4.15E-11	4.07E-11	1.00E-10	9.99E-08	401	32
	C3	6.50E-11	6.54E-11	6.68E-11	6.50E-11	1.00E-10	1.00E-07	271	22
	C4	5.25E-11	5.82E-11	5.36E-11	5.25E-11	1.00E-10	9.96E-08	347	28
S6	C1	4.36E-10	4.23E-10	4.15E-10	4.36E-10	1.00E-10	9.98E-08	123	9
	C2	4.78E-10	4.42E-10	4.61E-10	4.78E-10	1.00E-10	9.94E-08	123	10
	C3	2.49E-10	2.61E-10	2.61E-10	2.49E-10	1.00E-09	9.99E-08	482	41
	C4	4.47E-10	4.10E-10	4.66E-10	4.47E-10	1.00E-09	9.99E-08	501	44
S7	C1	4.46E-10	4.64E-10	4.48E-10	4.46E-10	1.00E-10	9.72E-08	125	13
	C2	1.76E-10	1.79E-10	2.02E-10	1.76E-10	1.00E-09	4.29E-08	159	17
	C3	1.82E-11	1.82E-11	1.74E-11	1.82E-11	1.00E-10	9.96E-08	456	53
	C4	5.82E-11	6.00E-11	5.85E-11	5.82E-11	1.00E-10	9.99E-08	426	51

In all seven scenarios with different cases of MHD-MCPNFF, the mean square error (MSE) between target data and output data for training, testing and validation processes is displayed in subfigures 3a-3g. The optimal precision and performance are approximately (10^{-10} to 10^{-11}) at 123, 290, 540, 371, 401, 123, and 456 epochs, respectively. Furthermore, the specific values of gradient and Mu appear to correspond to the step size of the back propagation of different cases for seven scenarios in MHD-MCPNFF, which are approximately (9.98×10^{-8}, 9.99×10^{-8}, 9.95×10^{-8}, 9.99×10^{-8}, 9.99×10^{-8}, 9.98×10^{-8} and 9.99×10^{-8}) and (10^{-10}), as shown in subfigures 4a-4g. These plots demonstrate the convergen ce of LMBLA for every scenario in MHD-MCPNFF. The results of error histograms, which further investigate the patterns of error for each output and target data, are displayed in subfigures 5a–5g for MHD-MCPNFF. For each of the seven scenarios in a variety of cases, the zero axes and error box are approximately (-5.8×10^{-6}, -6.4×10^{-7}, -3.4×10^{-7}, -2.2×10^{-6}, 2×10^{-7}, -4.8×10^{-6} and 4.68×10^{-6}). The effectiveness of LMBLA for MHD-MCPNFF is illustrated in Figure 6 by the regression study and correlation analysis of the errors between the target and output data, which is proven by a correlation value R = 1 in the testing, validation, and training processes. Figure (7) depicts the accuracy of the LMBLA-based outputs generated, which are further validated by error graphs and target results obtained from the Lobatto IIIA numerical solver for all scenarios of MHD-MCPNFF. For various cases of the MHD-MCPNFF system, the largest errors for training, testing, and validation data of the LMBLA are around 5×10^{-5}, 2×10^{-5}, 5×10^{-6}, 2×10^{-5}, 1×10^{-5}, 5×10^{-5} and 2×10^{-5}.

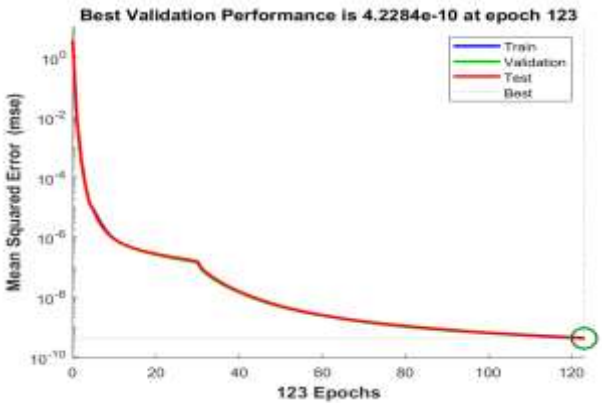

Fig. (3a): S1-C1: MSE outcomes

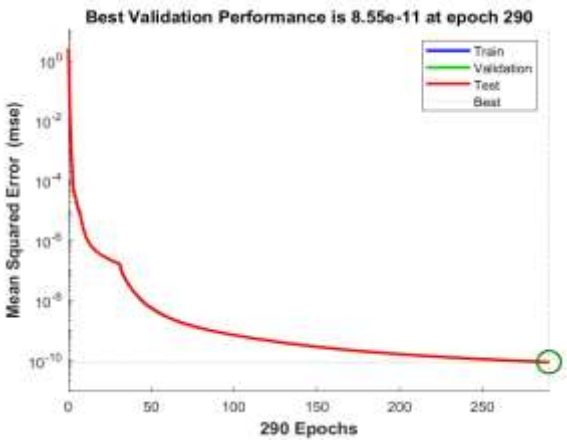

Fig. (3b): S2-C2: MSE outcomes

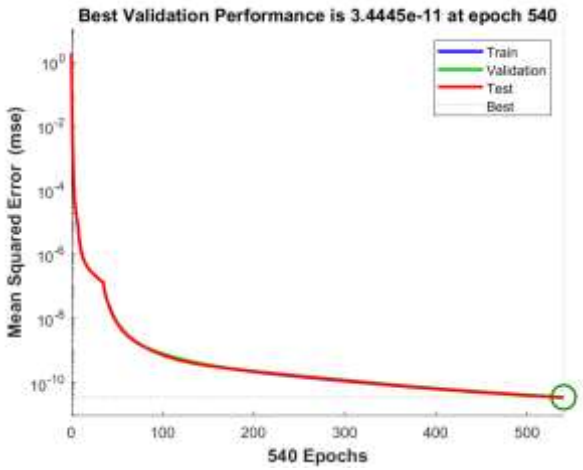

Fig. (3c): S3-C4: MSE outcomes

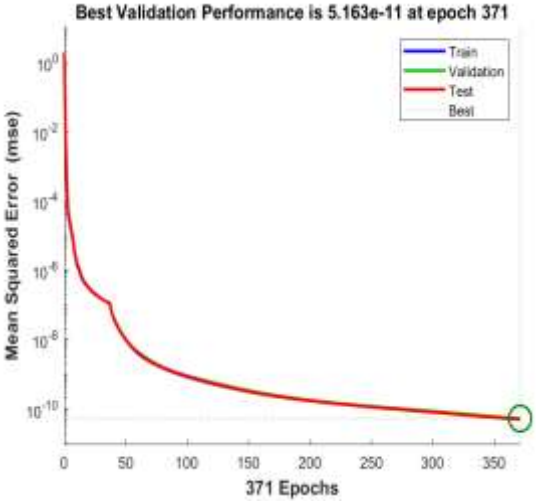

Fig. (3d): S4-C4: MSE outcomes

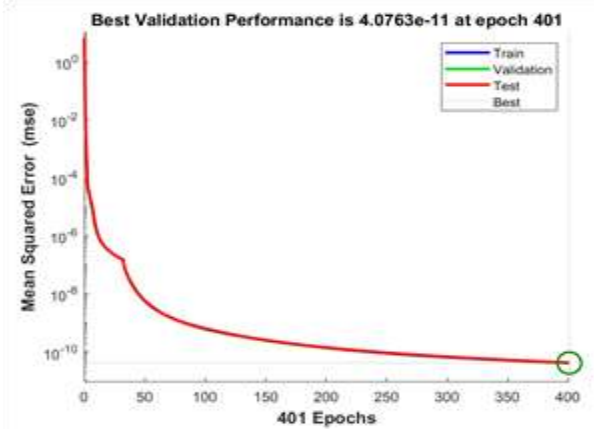

Fig. (3e): S5-C2: MSE outcomes

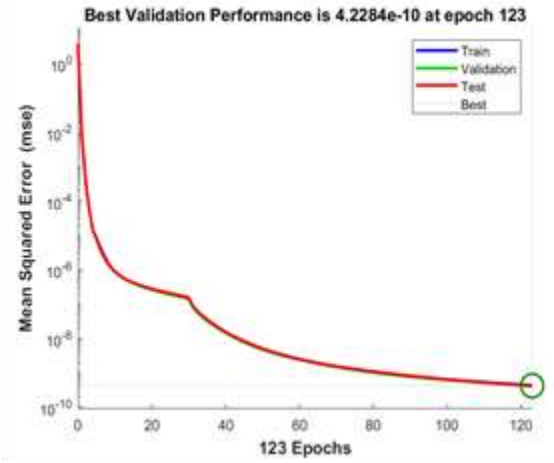

Fig. (3f):S6-C1: MSE outcomes

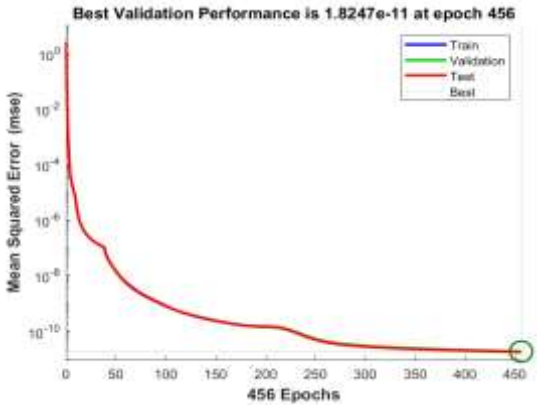

Fig. (3g): S7-C3: MSE outcomes

Fig. (3): LMBLA performance outcomes for various cases of MHD-MCPNFF

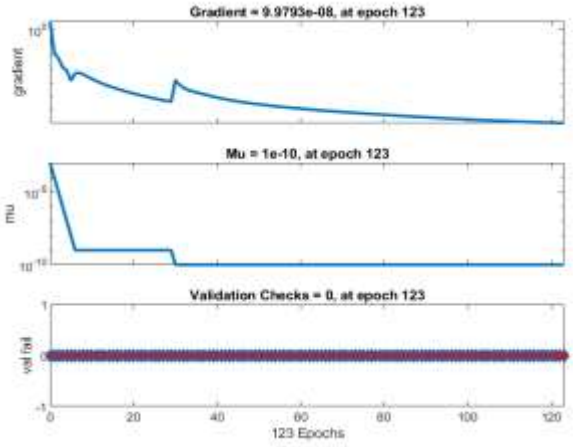

Fig. (4a): S1-C1: Transition state study

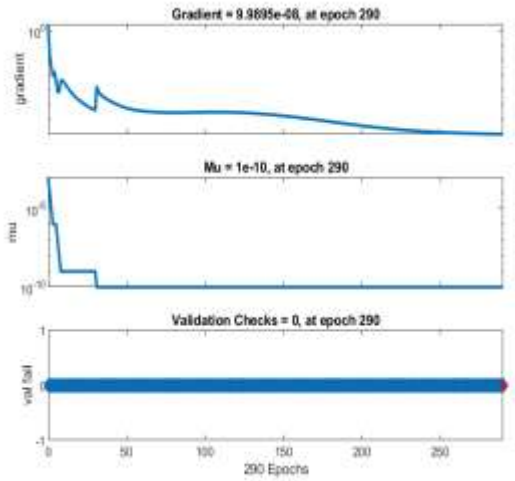

Fig. (4b): S2-C2: Transition state study

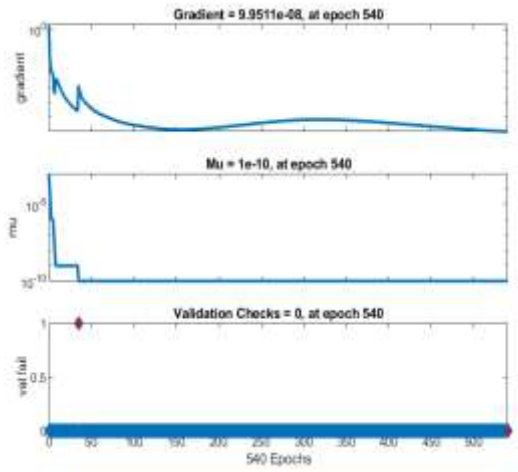

Fig. (4c): Transition state study

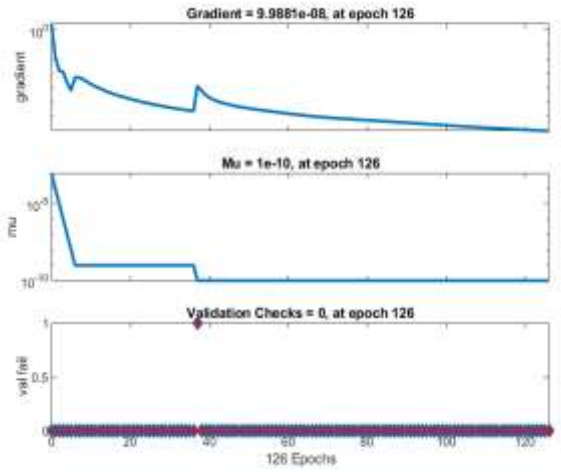

Fig. (4d): S4-C1: Transition state study

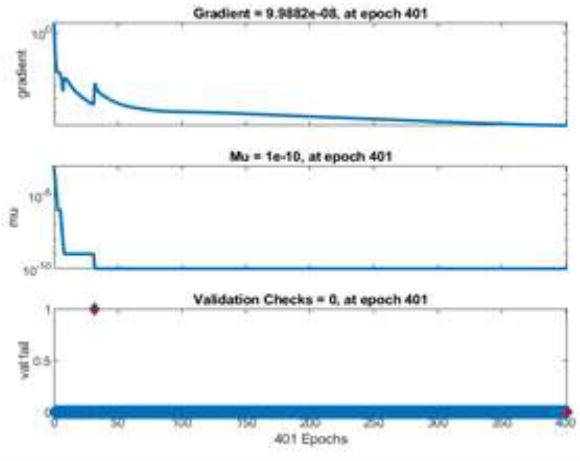

Fig. (4e): S5-C2: Transition state study

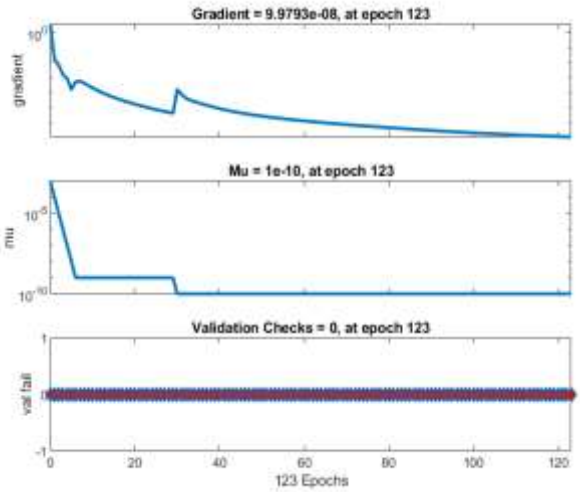

Fig. (4f): S6-C1: Transition state study

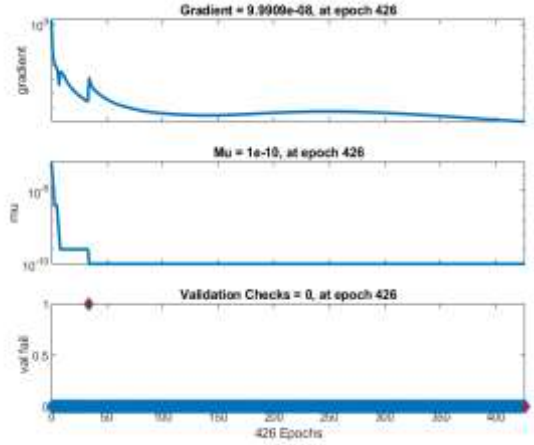

Fig. (4g): S7-C4: Transition state study

Fig. (4): LMBLA transition state study for various cases of MHD-MCPNFF

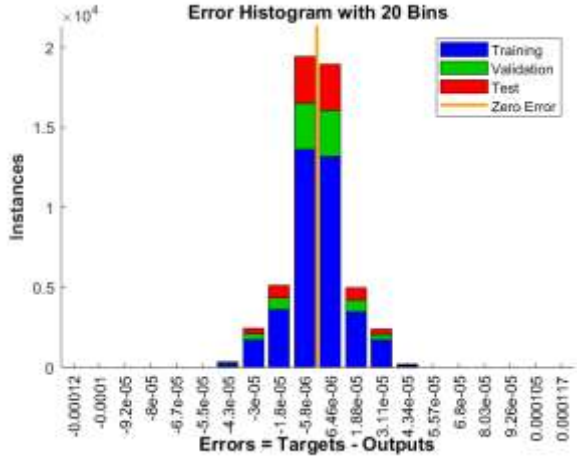

Fig. (5a): S1-C4: Error histogram representation

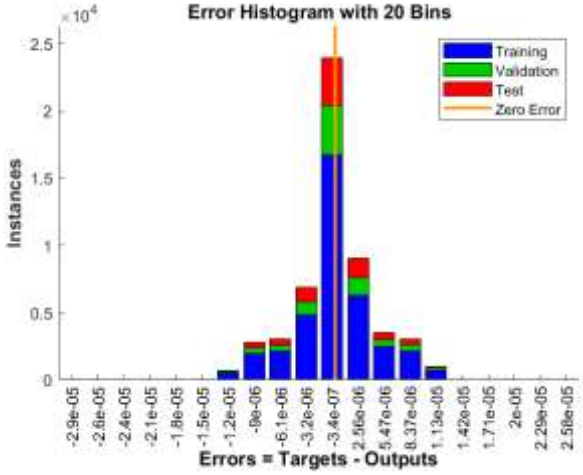

Fig. (5c): S3-C3: Error histogram representation

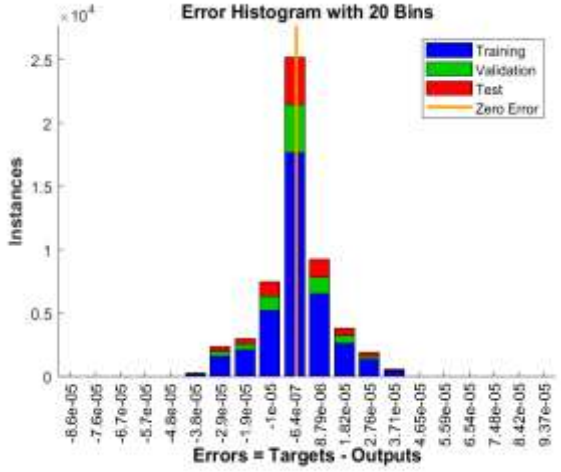

Fig. (5b): S2-C3: Error histogram representation

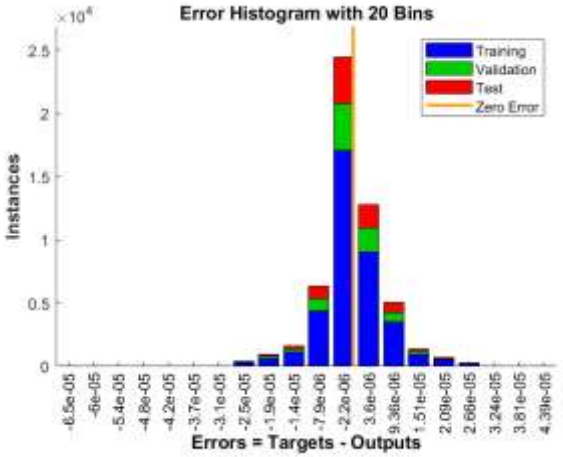

Fig. (5d): S4-C4: Error histogram representation

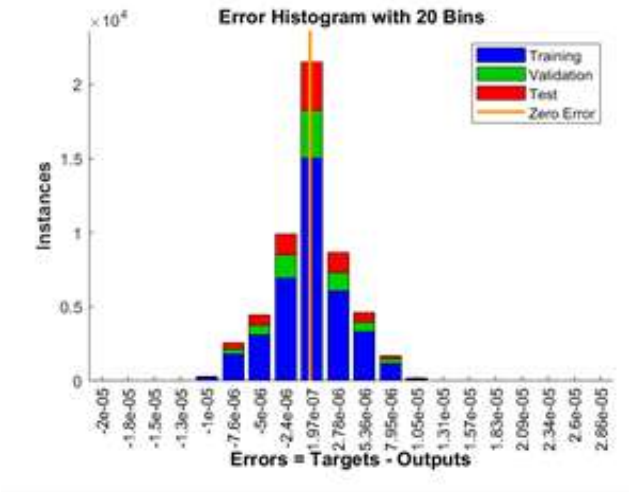

Fig. (5e): S5-C1: Error histogram representation

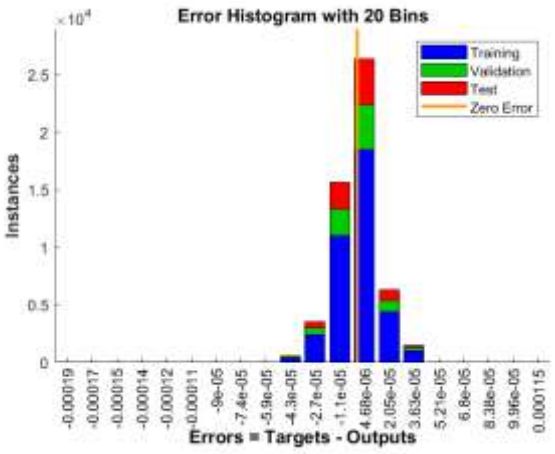

Fig. (5g): S7-C2: Error histogram representation

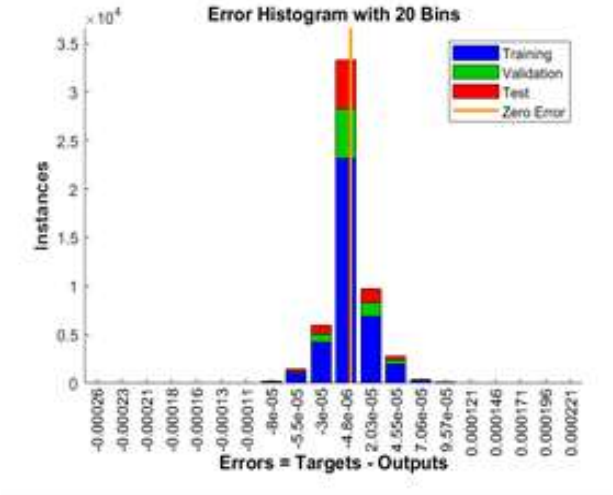

Fig. (5f): S6-C4: Error histogram representation

Fig. (5): LMBLA error histogram representation for various cases of MHD-MCPNFF

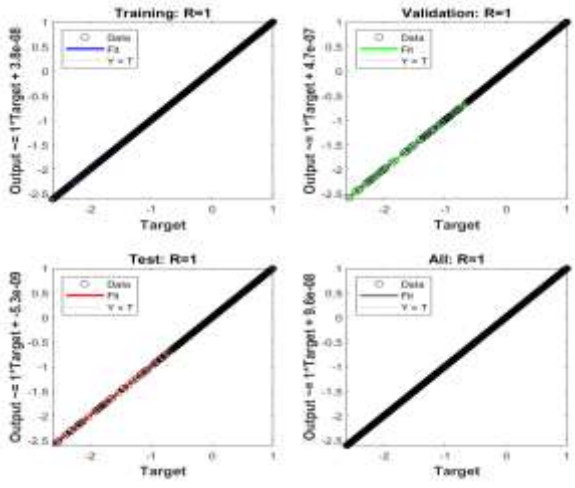

Fig. (6a): S1-C1: Regression illustration

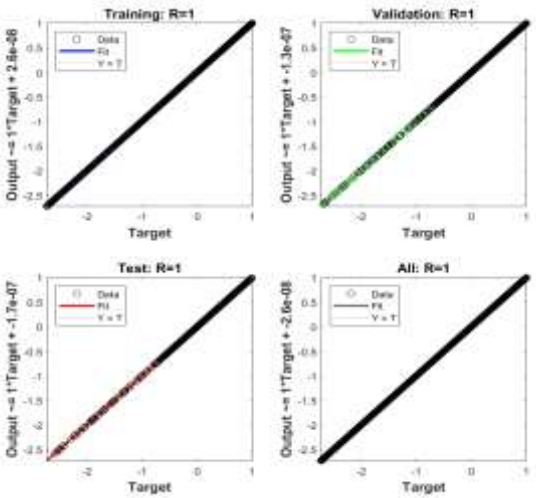

Fig. (6b): S2-C2: Regression illustration

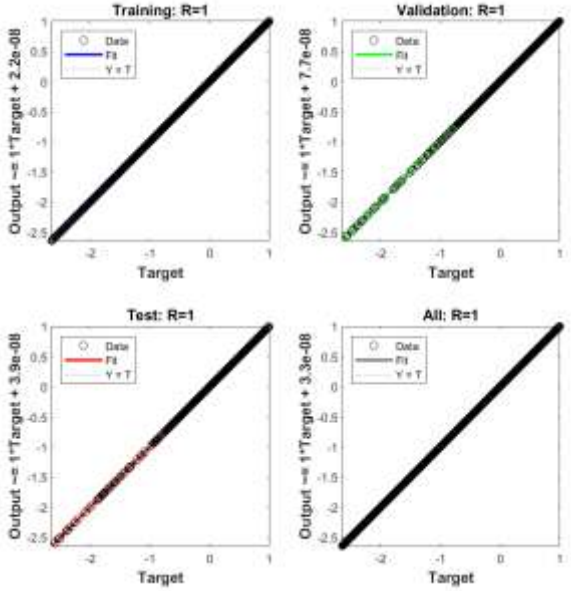

Fig. (6c): S3-C3: Regression illustration

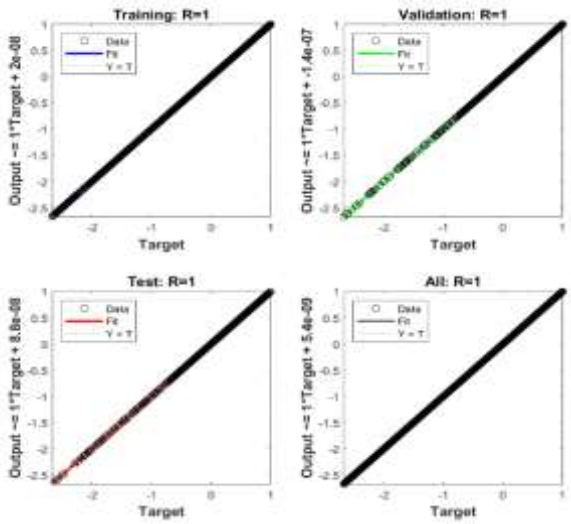

Fig. (6d): S4-C4: Regression illustration

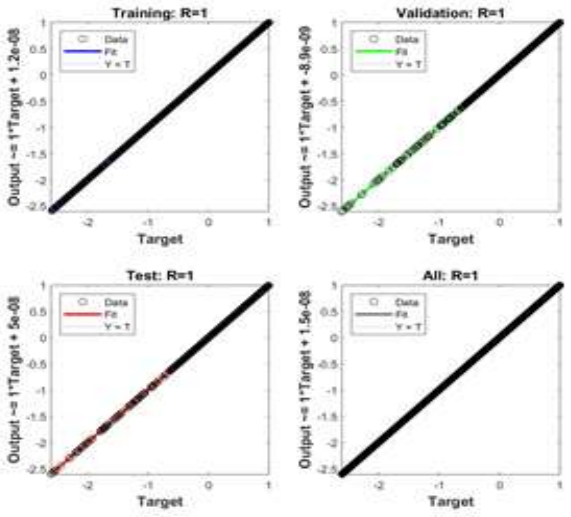

Fig. (6e): S5-C1: Regression illustration

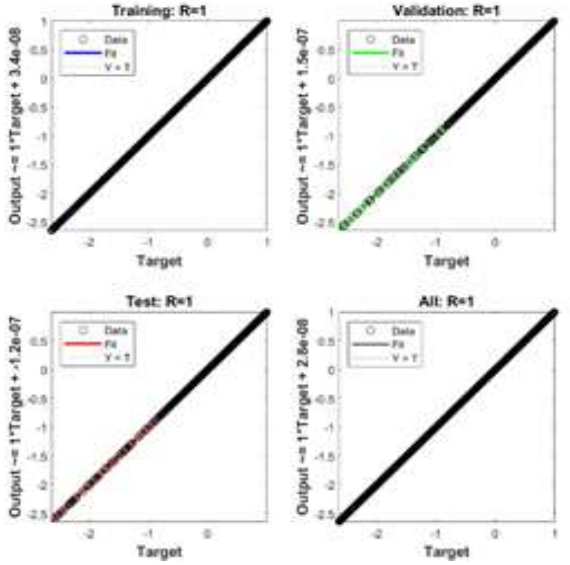

Fig. (6f): S6-C2: Regression illustration

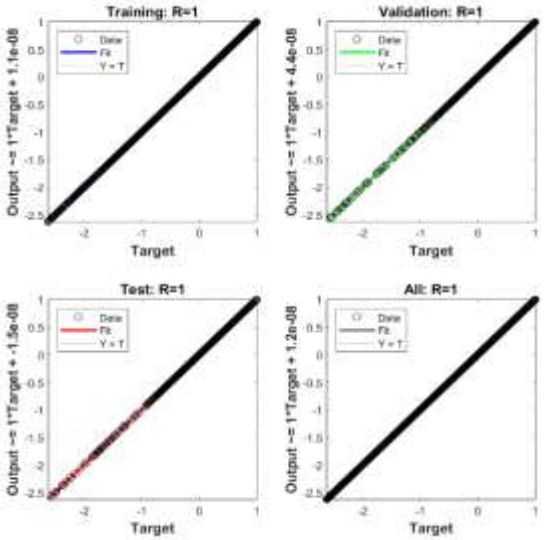

Fig. (6g): S7-C3: Regression illustration

Fig. (6): LMBLA regression illustration for various cases of MHD-MCPNFF

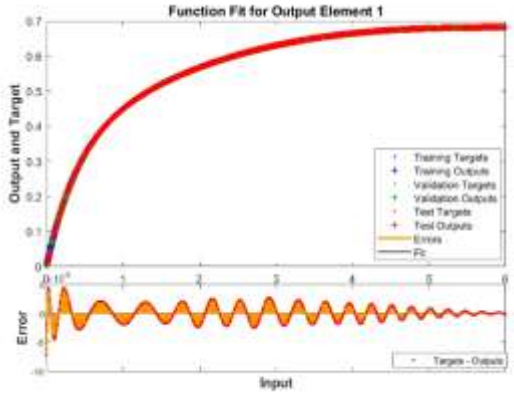

Fig. (7a): S1-C2: Fitting description

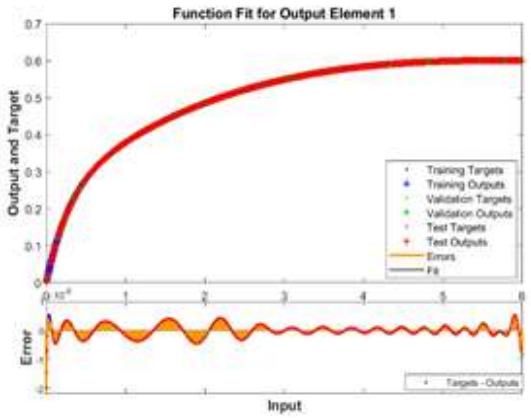

Fig. (7e): S5-C1: Fitting description

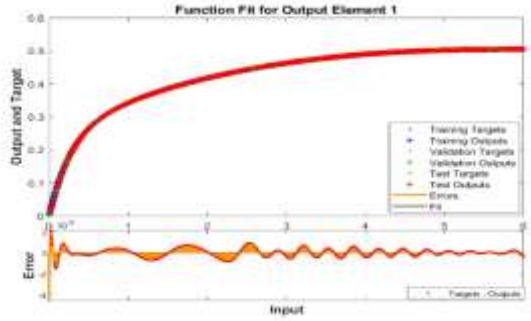

Fig. (7b): S2-C3: Fitting description

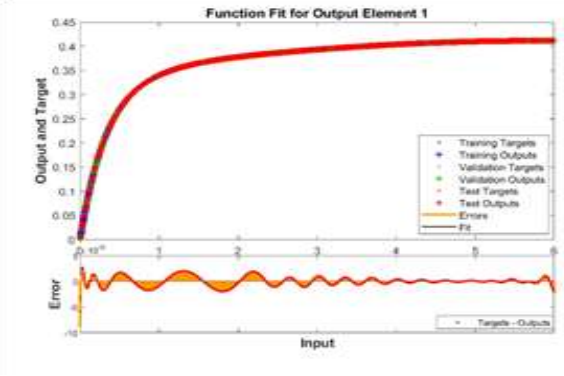

Fig. (7f): S6-C3: Fitting description

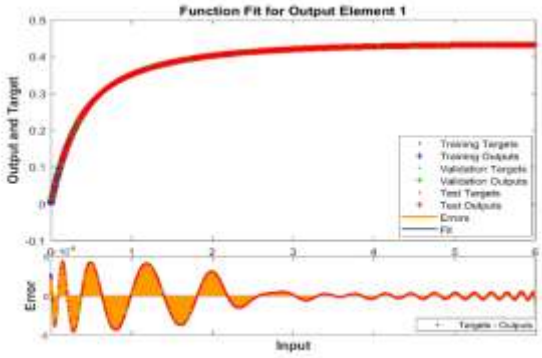

Fig. (7c): S3-C3: Fitting description

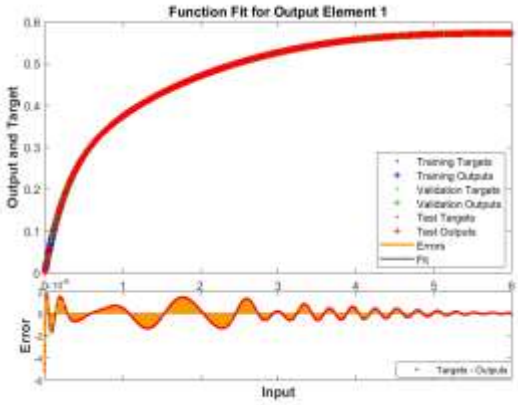

Fig. (7g): S7-C2: Fitting description

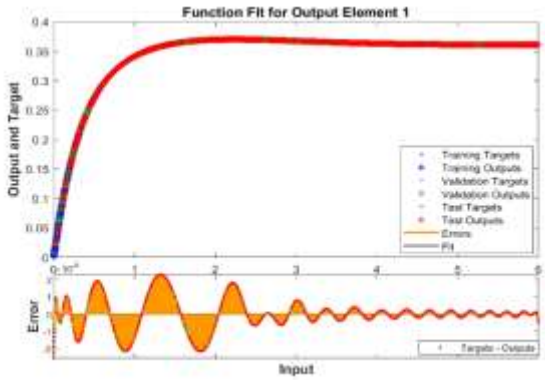

Fig. (7d): S4-C2: Fitting description

Fig. (7): LMBLA fitting description for various cases of MHD-MCPNFF

Figures 8-11 display the numerical solutions of the MHD-MCPNFF model by LMBLA which represent the effects of the different values of physical parameters such as the Prandtl fluid (α), magnetic parameter (M), Brownian motion (Nb), thermophoresis (Nt), activation energy (E), the reaction rate (σ), and Peclet number (Pe) on the behavior changes of the flow velocity f', temperature distribution θ, nanoparticle concentration φ, and microorganisms motile density χ. Sub-figures 8a-8b are illustrations of the effects of the Prandtl fluid and magnetic parameters on the flow velocity, which is the increasing value of the Prandtl fluid parameter causes the rising of the flow velocity while the flow velocity is decreased for the growing rates of magnetic parameter. Physically, the increase in Prandtl fluid parameter values implies reduced fluid viscosity and that leads to the flow velocity being raised. Also, the rising of a magnetic parameter generates resistive force and this causes the decreasing flow velocity. As shown in Figure 9, the fluid temperature rises with larger quantities of thermophoresis and Brownian motion. The physical meaning of that is the enhanced Brownian motion and thermophoresis characteristics cause the increasing internal motion energy of the nanoparticles and this implies increasing heat transmission and temperature distribution. Figure 10 demonstrates that the nanoparticle concentration has the opposite behavior for growing values of activation energy parameter and chemical reaction rate. In physics, higher values of chemical reaction rate are associated with more destructive chemical reactions that effectively eliminate fluid species. Furthermore, the increased activation energy parameter deprecates the modified Arrhenius function that supports the generated chemical process. The growth of the Peclet number reasons the enhanced diffusivity for microorganisms and this implies that the motile density is decreasing, as plotted in Fig. (11).

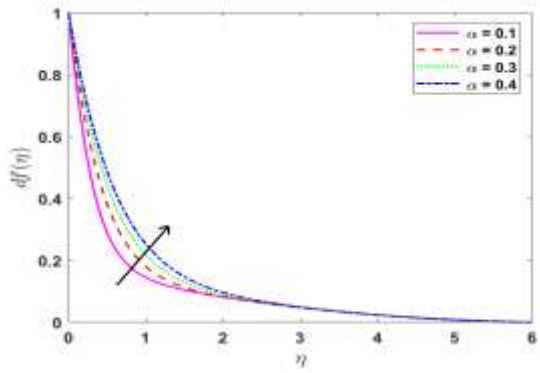

Fig. (8a): Variants of f' for α

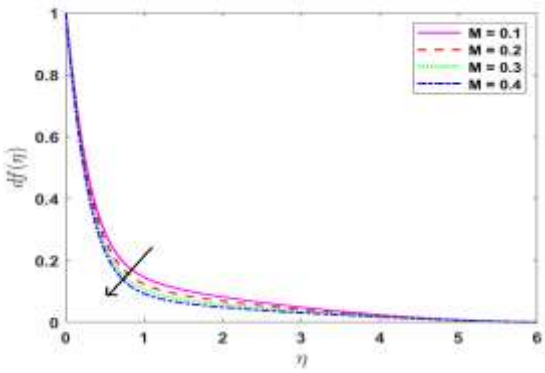

Fig. (8b): Variants of f' for M

Fig. (8): The variants of flow velocity for the Prandtl fluid parameter and magnetic parameter

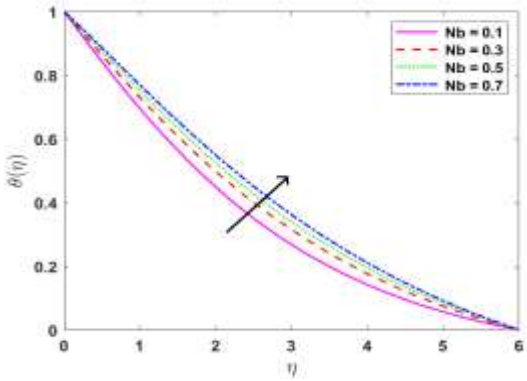

Fig. (9a): Variants of θ for Nb

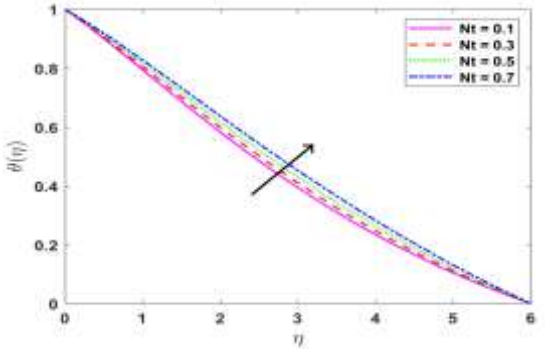

Fig. (9b): Variants of θ for Nt

Fig. (9): Variants of temperature distribution for Brownian motion and thermophoresis

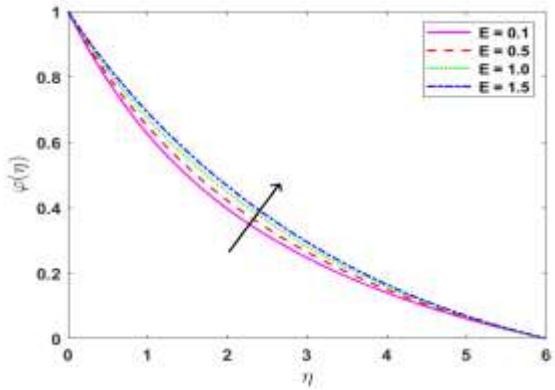

Fig. (10a): Variants of φ for E

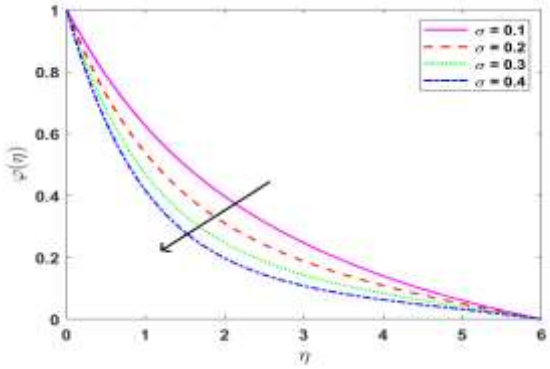

Fig. (10b): Variants of φ for σ

Fig. (10): Variants of nanoparticle concentration for activation energy parameter and chemical reaction rate

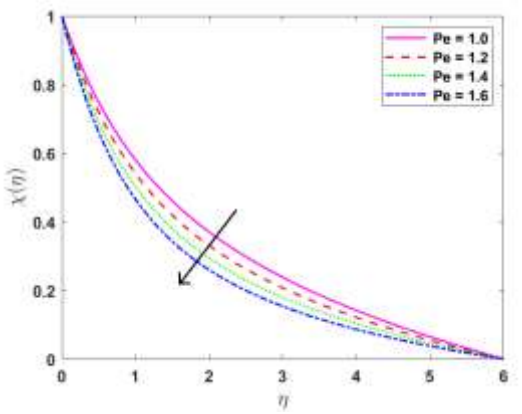

Fig. (11): Variants of microorganisms motile density for Peclet number

Conclusion and Recommendations

In this work, the designed Levenberg-Marquardt backpropagation learning algorithm LMBLA was used for studying the flow features of the magnetohydrodynamic mixed convective flow of Prandtl nanofluid MHD-MCPNFF with gyrotactic microorganisms influenced by activation energy across a stretchable surface. The non-linear partial differential equations PDEs system that represents the MHD-MCPNFF was transmuted into a dimensionless non-linear ordinary differential equations ODEs system. The Lobato IIIA approach was employed to construct the data set for designing LMBLA by solving ODEs for different physical parameters. The suggested LMBLA with 20 hidden neurons is created using 75%, 15%, and 15% of the data set chosen for training, testing, and validation steps.

The basic outcomes of this study are

- The convergence of the designed LMBLA for MHD-MCPNFF is shown through the gradient outcomes and Mu variable values of 10^{-8} to 10^{-10}.
- The accuracy of the proposed LMBLA for MHD-MCPNFF is represented through error analysis plots such as MSE, error histograms, and fitting illustrations, which the errors between 10^{-6} to 10^{-11}.
- The flow velocity is rising for large values of the Prandtl fluid parameter while it decreases with the increasing magnetic parameter rate.
- For growing values of Brownian motion and thermophoresis, the fluid temperature is rising.
- The nanoparticle concentration has opposite behavior for high rates of activation energy and chemical reaction rate.
- The rising value for the Peclet number leads to a decrease in the motile density.

Finally, Since the designed LMBLA proved effective and accurate in this study, It can be used for many problems of the nanofluid influenced by the activation energy **(Jawad et., 2023; Taj and Salahuddin, 2023)** in future work.

Acknowledgment

This research work was funded by Institutional Fund Projects under grant no. (IFPIP: 926-247-1443). The authors gratefully acknowledge technical and financial support provided by the Ministry of Education and King Abdulaziz University, DSR, Jeddah, Saudi Arabia.

References

Ahmed, F., Reza-E-Rabbi, S., Ali, M. Y., Ali, L. E., Islam, A., Rahman, M. A., and Ahmmed, S. F. (2024). *Numerical modeling of a MHD non-linear radiative Maxwell nano fluid with activation energy*. Heliyon.

Al-Yaari, A., Ching, D. L. C., Sakidin, H., Muthuvalu, M. S., Zafar, M., Haruna, A., and Jagaba, A. H. (2023). The effects of nanofluid thermophysical properties on enhanced oil recovery in a heterogenous porous media. *Case Stud. Chem. Environ. Eng.*, 100556.

Asad, S., and Riaz, S. (2023). Analysis of entropy generation and nonlinear convection on unsteady flow of MHD Prandtl fluid with Soret and Dufour effects. *Arab. J. Math.*, *12*(1), 49-69.

Asghar, S. A., Ahmad, I., Ilyas, H., Abdullah, M., Shoaib, M., and Raja, M. A. Z. (2024). Numerical treatment of singular functional systems in quantum calculus: adaptive backpropagated Levenberg–Marquardt neural networks. *Eur. Phys. J. Plus*, *139*(1), 10.

Bafakeeh, O.T., Raghunath, K., Ali, F., Khalid, M., Tag-ElDin, E.S.M., Oreijah, M., Guedri, K., Ben Khedher, N., and Khan, M.I. (2022). Hall Current and Soret Effects on Unsteady MHD Rotating Flow of Second-Grade Fluid through Porous Media under the Influences of Thermal Radiation and Chemical Reactions. *Catal.*, *12*, 1233.

Choi, S. U., and Eastman, J. A. (1995). Enhancing thermal conductivity of fluids with nanoparticles (No. ANL/MSD/CP-84938; CONF-951135-29). *Argonne National Lab. (ANL)*, Argonne, IL (United States).

Galal, A. M., Alharbi, F. M., Arshad, M., Alam, M. M., Abdeljawad, T., and Al-Mdallal, Q. M. (2024). Numerical investigation of heat and mass transfer in three-dimensional MHD nanoliquid flow with inclined magnetization. *Sci. Rep.*, *14*(1), 1207.

Goud, J. S., Srilatha, P., Kumar, R. V., Sowmya, G., Gamaoun, F., Nagaraja, K. V., and Eldin, S. M. (2023). Heat transfer analysis in a longitudinal porous trapezoidal fin by non-Fourier heat conduction model: An application of artificial neural network with Levenberg–Marquardt approach. *Case Stud. Therm. Eng.*, *49*, 103265.

Hafeez, A., Aldosari, F. M., Helmi, M. M., Ghazwani, H. A., Hussien, M., and Hassan, A. M. (2023). Heat transfer performance in a Hybrid nanofluid (Cu-Al2O3/kerosene oil) flow over a shrinking cylinder. *Case Stud. Therm. Eng.*, *52*, 103539.

Jabeen, K., Mushtaq, M., Mushtaq, T., and Muntazir, R. M. A. (2024). A numerical study of boundary layer flow of Williamson nanofluid in the presence of viscous dissipation, bioconvection, and activation energy. *Nume. Heat Transf.*, Part A: Applications, *85*(3), 378-399.

Jawad, M., Hameed, M. K., Nisar, K. S., and Majeed, A. H. (2023). Darcy-Forchheimer flow of maxwell nanofluid flow over a porous stretching sheet with Arrhenius activation energy and nield boundary conditions. *Case Stud. Therm. Eng.*, *44*, 102830.

Kumar, K.G., Haq, R.U., Rudraswamy, and N., Gireesha, B. (2017). Effects of mass transfer on MHD three dimensional flow of a Prandtl liquid over a flat plate in the presence of chemical reaction. *Results Phys*, *7*, 3465–3471.

Mahmood, Z., Eldin, S. M., Rafique, K., and Khan, U. (2023). Numerical analysis of MHD tri-hybrid nanofluid over a nonlinear stretching/shrinking sheet with

heat generation/absorption and slip conditions. *Alex. Eng. J., 76*, 799-819.

Modi, K. V., Patel, P. R., and Patel, S. K. (2023). Applicability of mono-nanofluid and hybrid-nanofluid as a technique to improve the performance of solar still: A critical review. *J. Clean. Prod.*, 135875.

Mukdasai, K., Sabir, Z., Raja, M. A. Z., Sadat, R., Ali, M. R., and Singkibud, P. (2022). A numerical simulation of the fractional order Leptospirosis model using the supervise neural network. *Alex. Eng. J., 61*(12), 12431-12441.

Reddy, Y. D., Goud, B. S., Nisar, K. S., Alshahrani, B., Mahmoud, M., and Park, C. (2023). Heat absorption/generation effect on MHD heat transfer fluid flow along a stretching cylinder with a porous medium. *Alex. Eng. J., 64*, 659-666.

Selim, M. M., El-Safty, S., Tounsi, A., and Shenashen, M. (2023). Review of the impact of the external magnetic field on the characteristics of magnetic nanofluids. *Alex. Eng. J., 76*, 75-89.

Shah, Z., Shafiq, A., Rooman, M., Alshehri, M. H., and Bonyah, E. (2023). Darcy Forchhemier Prandtl-Eyring nanofluid flow with variable heat transfer and entropy generation using Cattaneo-Christov heat flux model: Statistical approach. *Case Stud. Therm. Eng., 49*, 103376.

Taj, M., and Salahuddin, T. (2023). Analysis of viscously dissipated three-dimensional flow of Williamson fluid with nonlinear radiation and activation energy. *Alex. Eng. J., 76*, 595-607.

Waqas, H., Khan, S. A., Ali, B., Liu, D., Muhammad, T., and Hou, E. (2023). Numerical computation of Brownian motion and thermophoresis effects on rotational micropolar nanomaterials with activation energy. *Propuls. Power Res., 12*(3), 397-409.

Yasir, M., Khan, M., Al-Zubaidi, A., and Saleem, S. (2023). Arrhenius activation energy effect in thermally viscous dissipative flow of micropolar material with gyrotactic microorganisms. *Alex. Eng. J., 84*, 204-214.

Zafar, S. S., Alfaleh, A., Zaib, A., Ali, F., Faizan, M., Abed, A. M., and Khan, M. I. (2023). Simulation of Prandtl Nanofluid in the Mixed Convective Flow of Activation Energy with Gyrotactic Microorganisms: Numerical Outlook Features of Micro-Machines. *Micromachines, 14*(3), 559.

تصميم خوارزمية تعلم الانتشارالعكسي لتدفق الحمل الحراري الهيدروديناميكي المغناطيسي المختلط لسوائل براندتل النانوية مع طاقة التنشيط

إيمان فايز الشهري[١] ، ا.د/ ايمان سالم العيدروس[١] ، ا.د/ رانيا الحربي[١] ، ا.د/ محمد اسف زاهور راجا[٢]

[١] قسم الرياضيات- كلية العلوم- جامعة الملك عبدالعزيز- جدة- المملكة العربية السعودية
[٢] مركز أبحاث تكنولوجيا المستقبل- جامعة يونلين الوطنية للعلوم والتكنولوجيا- دوليو- يونلين- تايوان

استخدام تقنيات الذكاء الاصطناعي في حل التحديات قد زادت شهرته مؤخرًا في مجموعة متنوعة من المجالات. بالإضافة إلى ذلك، يعتبر النانوفلويد مثير للاهتمام في مجموعة متنوعة من التطبيقات، خاصة في أنظمة التبريد ونقل الحرارة، حيث يتم استخدامه لتحسين الخصائص الحرارية للسائل. في هذه الورقة البحثية، يتم تقديم تصميم لخوارزمية تعلم الانتشار العكسي لتحليل خواص التدفق عند تدفق الحمل الحراري الهيدروديناميكي المغناطيسي المختلط لسوائل براندتل النانوية مع الكائنات الحية الدقيقة الميكروسكوبية على سطح مطاطي متأثر بطاقة التنشيط. يتم الحصول على نظام معادلات تفاضلية عادية من نظام معادلات تفاضلية جزئية للصيغة الرياضية الأصلية باستخدام تحويلات مناسبة. يتم تطبيق تقنية لوباتو IIIA لحل المعادلات التفاضلية العادية لسيناريوهات مختلفة من خلال تغيير قيم سائل براندلت (α)، معامل المغناطيسية (M)، حركة براونية (Nb)، الحركة الحرارية (Nt)، طاقة التنشيط (E)، معدل ردة الفعل الكيميائية (σ)، ومعامل بيكليت (Pe) للعثور على مجموعة من البيانات لنموذج التدفق. باستخدام هذه الحلول من خلال أداة nftool في ماتلاب لتصميم خوارزمية التعلم العكسي للوفنبرغ-ماركواردت. يتم التحقق من فعالية ودقة خوارزمية التعلم العكسي للوفنبرغ-ماركواردت المصممة من خلال متوسط الخطأ المربع وتوزيع الأخطاء ورسومات الانحدار التوضيحية. تتمتع سرعة التدفق بسلوك معاكس للقيم المتزايدة لمعاملات سائل براندتل والمغناطيسية. من أجل زيادة قيم حركة براونية وحركة التسخين الحراري، تزداد درجة حرارة السائل. تشير القيم المتزايدة لمعامل طاقة التنشيط إلى زيادة تركيز الجسيمات النانوية.